Optical and Quantum Electronics (2021) 53:511
https://doi.org/10.1007/s11082-021-03186-2

Computational analysis of chalcogenides as an inorganic hole transport layer in perovskite solar cells

Atul Kumar[1] · **Pranay Ranjan**[2,3]

Received: 5 April 2021 / Accepted: 5 August 2021 / Published online: 14 August 2021

Abstract
Fill factor (FF) deficit and stability is a primary concern and challenge with the perovskite solar cell. The band alignment and resistance at the junction interface further decreases the fill factor and thus limits the performance of the device. Moreover, degradation of the intrinsic properties of the upcoming perovskite material such as methylammonium lead halide on exposure to ambience or moisture creates instability and decreases the shelf life of the device. To overcome all these challenges, we have engineered the device structure and introduces an earth-abundant material in the primitive perovskite structure by introducing an inorganic hole transport layer (HTL). It was observed from the calculation that the FF is sensitive to the band offset values. Moreover, the band alignment/band offset role and effect at the Perovskite/HTL junction were investigated. It is evident from the calculation that the inorganic material replacing Spiro-MeOTAD can enhance the stability of the device by providing insulation from ambient. The efficiency of SnS and spiro-MeOTAD were found to be comparable in the present work and thus the shelf life and moisture sensitivity challenge of the perovskite solar cell is addressed. Moreover, this work paves the way for earth-abundant p-type chalcogenides tin selenide (SnS) as a HTL layer in the perovskite solar cell.

Keywords Perovskite · Inorganic HTL · Chalcogenide · SCAPS Simulation

1 Introduction

Terawatt scale perennial supply of pollution-free energy at a competitive cost is a necessity and demand for sustainable growth. Photovoltaic is amongst one of the potential solution subjected to the availability of low cost, nontoxic material, and fabrication technology. Perovskite methylammonium lead halide ($CH_3NH_3PbI_3$ or $MAPbI_3$) possesses enhanced properties such as light absorption, optimal defect-free bandgap, high mobility and diffusion

✉ Atul Kumar
er.atul89@gmail.com

[1] ECE Department, KL University, Guntur, Andhra Pradesh 522502, India

[2] Department of Physics, UAE University, Al-Ain-1555, UAE

[3] National Water and Energy Center, UAE University, Al-Ain-15551, UAE

length. Ever since its inception, in a very short span perovskite solar cell has dominated the solar industries due to its high a power conversion efficiency of 22.1% (Green et al. 2017). However, the small shelf life of the perovskite materials and sensitivity to ambience conditions such as moisture, temperature and photosensitivity remains a hindrance to its path for industrial production (Wang et al. 2016; Hwang et al. 2015). Organic material such as MA (methylammonium), is used for device fabrication in perovskite solar cell and is extremely sensitive to water or humidity and gets degraded upon exposure. Thus, it leads to degradation of the device performance and efficiency. Tin selenide an earth-abundant, low-cost and non-toxic material is one of the possible replacement for the organic MA as it's insensitive to moisture and can act as a passivation layer. Moreover, the encapsulation of the organic layer by the use of inorganic material such as titanium dioxide (TiO_2) as electron transport layer (ETL) on one side and another inorganic material SnS as hole transport layer (HTL) on the other side of the organic material enhances the shelf life of the device by shielding it from humidity, elevated temperature and photodegradation. In comparison to polymers HTL such as Spiro-MeOTAD, PEDOT: PSS etc. which have low mobility of holes, instability issues (thermal, UV and moisture stability) and high-cost, inorganic layers (SnS and TiO_2) are cost-effective, stable and robust under thermal, UV and moisture exposure. Some of the inorganic materials which are reported as HTL application in perovskite solar cell in literature are listed in Table 1. To find a probable replacement of these listed HTL materials in Table 1 we have explored inorganic chalcogen materials (CIGS, CZTS, SnS, Cu_2S, PbS, Sb_2S_3, FeS_2) for HTL, where all the elements are nontoxic, and earth-abundant (Mitzi et al. 2013) and can be economically processed for solar cell application. The *p*-type nature of these chalcogens with high acceptor density and hole mobility has the potential to overcome other reported inorganic materials for HTL application. In addition, the low thermal conductivity and resilient to the ambient condition further makes the inorganic layer a promising candidate for upcoming perovskite solar cell. To discuss and gain some insight into the feasibility of inorganic HTL here, we performed a simulation study with an inorganic hole transport layer in perovskite.

1.1 Chalcogens

Chalcogens, selected here (CIGS, CZTS, SnS, Cu_2S, PbS, Sb_2S_3, FeS_2) are prominent p-type absorber material with high absorption coefficient ($\sim 10^5$ cm^{-1}) and bandgap lying in visible region (0.5–1.5 eV) (Yu et al. 2016; You et al. 2016; Dhingra et al. 2016; Lv et al. 2015; Qin et al. 2014; Xu et al. 2017; Wu et al. 2015; Gokmen et al. 2013; Shin et al. 2013; Burton

Table 1 The reported inorganic HTL in perovskite solar cell in literature

	V_{OC} (V)	J_{SC} (mA/cm^2)	FF (%)	Eff. (%)
Cu_2O (Yu et al. 2016)	0.952	17.5	66.2	11.03
NiO (You et al. 2016)	1.01	21	76	16.1
CuI (Dhingra et al. 2016)	0.55	17.8	62	6
$CuInS_2$ (Lv et al. 2015)	0.878	16.6	45.1	6.57
CuSCN (Qin et al. 2014)	1.020	19.2	58	11.4
CIGS (Xu et al. 2017)	0.94	17.66	54.88	9.15
CZTS (Wu et al. 2015)	1.06	20.54	58.7	12.75
PbS (Dhingra et al. 2016)	0.86	12.1	72	7.5

et al. 2013; Skelton et al. 2015; Lim et al. 2009; Tang 2017; Yeon et al. 2015; Wei 2014; Angelis et al. 2016; Altermatt et al. 2002; Popov et al. 2013). The material properties of all the chalcogens were listed in Table 2. These are earth-abundant materials available enough for terawatt scale energy generation and are non-toxic as well as cost-effective. The synthesis and solution-processed fabrication techniques make them advantageous for low-cost application. These chalcogens are also called multifunction material due to their application ranging from (i) Prominent absorber layer in inorganic and hybrid solar cells, (ii) Counter electrode in DSSC and batteries, (iii) Photocatalyst, (iv) as a gas sensor (v) Counter electrode in quantum dot solar cell, (vi) Thermoelectric (vii) Ultra-fast photo-detector and optoelectronic applications. It is to be noted that, all chalcogens used here are in binary (SnS, Cu_2S, PbS, Sb_2S_3, FeS_2) and quaternary (CIGS, CZTS) phases for enhanced hole mobility in comparison to Spiro-MeOTAD.

2 Simulation details

Solar cell capacitance simulator (SCAPS-1D) version 3.3.0.2 is used for the theoretical study (Burgelman et al. 2000; Kumar 2021a, 2021b, 2021c; Kumar and Ranjan 2021, 2020). SCAPS model semiconductor and electrostatic equation in the 1D environment is utilized to simulate a thin-film solar cell. Newton Raphson and Gummel iteration was implemented to solve the 1D Poisson equation and continuity equation for heterostructures. To begin with, we have modelled a *p-i-n* structure FTO/TiO_2/$MAPbI_3$/Spiro-MeOTAD and simulated the performance of the solar cell. The reported material parameters of perovskite were thickness ~ 350 nm, bandgap ~ 1.55 eV, dielectric constant ~ 10, N_A as ~ 10^{13}/cm^3, the diffusion length of electrons in perovskite as L_p ~ 1000 nm. We have used electron mobility of ~ 10 cm^2/Vs, radiative recombination coefficient (cm^3/s) ~ 10^{-13}, the neutral defect density of ~ 10^{14} at the centre of the bandgap with a Gaussian distribution and characteristic energy of 0.1 eV; as well as the capture cross-section of electrons and holes as 2×10^{-14} cm^{-2}. The absorption constant A (1/cm eV^(½)) is assumed to be 10^5. The device is illuminated from the FTO layer side with AM1.5 spectrum using relevant SCAPS option at temperature 300 K. Front contact were made from the FTO layer and a back contact was taken from the metal contact with work function taken of 5.1 eV. For the series resistance (R_s) and shunt resistance (R_{sh}), we have used typical values of 5 Ω cm^2 and 5 k Ω cm^2. The schematic of the device is shown in Fig. 1a.

The relevant material parameters used in the simulation were obtained from the literature and are listed in Table 3 (Minemoto and Murata 2015; Hossain et al. 2015; Casas et al. 2017). The Quantum efficiency (QE) curve shows the maximum light absorption is within the perovskite layer. The simulated output parameter (V_{OC} = 1.08 V, J_{SC} = 24.5 mA/cm^2, FF = 75.5%, Efficiency = 20.02%) as shown in Fig. 1b are closely matching with the experimentally reported values of V_{OC}, J_{SC}, FF and efficiency (Yang et al. 2015). In addition, the bandgap of the perovskite is 1.55 eV and the corresponding SQ limiting parameter are (V_{OC} 1.287 V, FF 90.32%, J_{SC} 26.37 mA/cm^2, Efficiency 30.68%).

3 Results and discussions

Design and configuration of the solar cell drives the mechanism of the photovoltaic action and efficiency. Structure optimization for an efficient separation and collection of photogenerated generated charge carrier ae some of the most important parameters. (a) Built-in

Table 2 Material property of selected chalcogenide for the inorganic hole transport layer

Parameters	CIGS (Gokmen et al. 2013)	CZTS (Gokmen et al. 2013; Shin et al. 2013)	SnS (Burton et al. 2013)	Cu_2S (Lim et al. 2009; Tang 2017)	PbS (Yeon et al. 2015; Wei 2014)	Sb_2S_3 (Angelis et al. 2016)	FeS_2 (Altermatt et al. 2002; Popov et al. 2013)
Hall mobility (cm^2/Vs)	~35	6–30	100	25	80	10	10
Thermal conductivity ($Wm^{-1}\ K^{-1}$) at room temperature	4.44 (Skelton et al. 2015)	1.69 (Skelton et al. 2015)	1.25	0.3–0.5	2.19	–	45
Band gap (eV)	1.13	1.5	1.5	1.2	0.92	1.7	0.95
Hole density (cm^{-3})	~10^{16}	~10^{14}–10^{17}	~10^{17}	~10^{19}	$10^{15}10^{17}$	~10^{16}	~10^{18}
Conductivity type	p	p	p	p	p	p	p
Electron Affinity (eV)	4.58	4.2	3.9–4.2	4.25	3.95	3.95	3.9

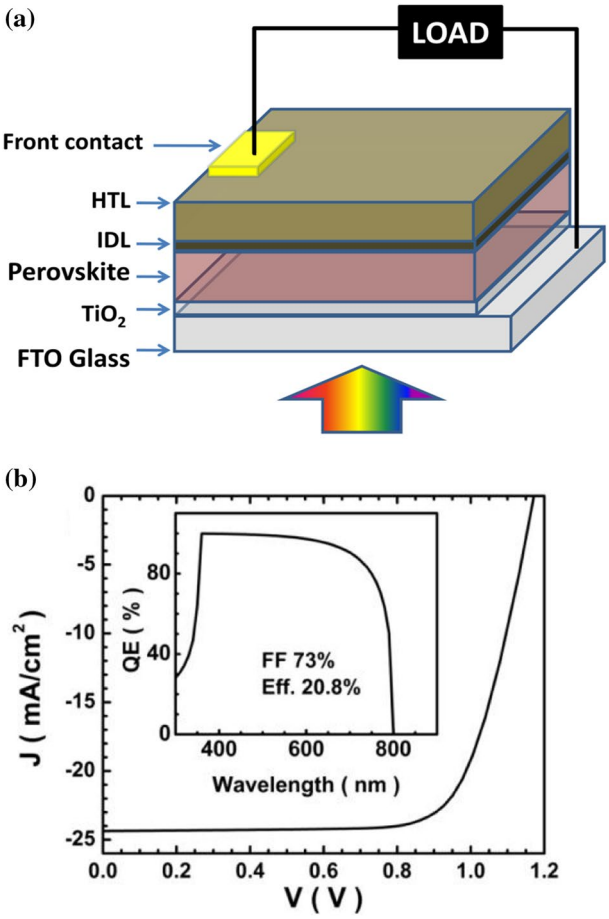

Fig. 1 **a** Schematic of the perovskite solar cell. **b** Simulated I-V and QE of perovskite solar cell

Table 3 List of material parameters used in the simulation

Parameters	TiO_2	SpiroMeOTAD	Perovskite
Thickness (nm)	100	190	350
Bandgap (eV)	1.5	3	1.55
Electron affinity (eV)	3.6	2.2	3.9
Dielectric permittivity	10	3	10
CB effective density of state N_C (cm^{-3})	2.2×10^{18}	2.8×10^{19}	2.2×10^{18}
VB effective density of state N_V (cm^{-3})	1.8×10^{19}	$1.\times10^{19}$	1.8×10^{19}
Electron thermal velocity (cm/s)	10^7	10^7	10^7
Hole thermal velocity (cm/s)	10^7	10^7	10^7
Electron/hole mobility (cm^2/Vs)	10	.0001/.0039	10/10
Donor/Acceptor density, N_D/N_A (cm^{-3})	10^{17}	10^{18}	10^{13}

electric field, (b) effective force field (work function difference), (c) discontinuity at an energy level at the interface, are some of the design-related parameters which are implemented for better performance of the photovoltaic device. The interface at heterojunction plays an important role as it controls the voltage generation, current flow, potential variation and the electric field at either side of the junction. The perovskite configuration of FTO/TiO_2/Perovskite/HTL is basically a *p-i-n*-type and this kind of *p-i-n* structures are in general suitable for the large built-in potential across absorber layer due to the dependence of built-in potential on the carrier density of *p* and *n* layer. The effective force field in such structures can be induced by the appropriate choice of the contacts work function. From the design point of view, an HTL should be having a high hole to electron mobility ratio so that it acts as a selective contact. Moreover, to increase the large built-in voltage, charge density should be higher in *n* and *p* region of *p-i-n* and this will lead to shift of the space charge layer into the intrinsic layer and thus will have higher charge density, an advantageous situation for charge drift. Figure 2a represents the higher built-in voltage resulting from the higher density of carrier in *p* and *n* layer. It was observed that the slope of band energy level in the *i* layer (absorber) increases with the carrier density in *p* and *n*. A spike is also present at the valence band offset to lower the interfacing recombination between $E_{V,\ HTM}$ and $E_{C,\ Perovskite}$ (Minemoto and Murata 2015; Rau and Schock 1999). The most

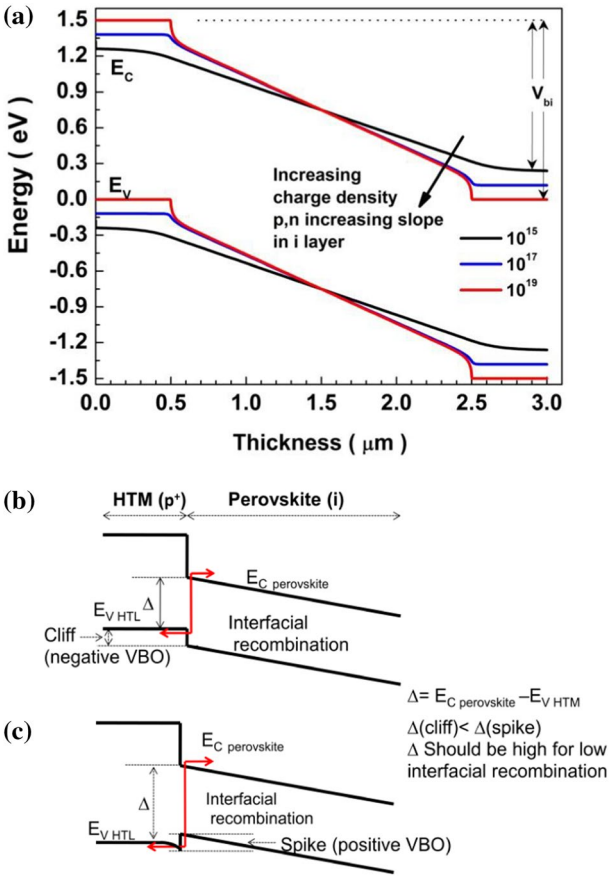

Fig. 2 **a** The *pin* junction shows a large built in voltage and slope of intrinsic (*i*) energy level in absorber increases with higher carrier density in *p* and *n* layer. **b** The Schematic of HTM/Perovskite band diagram. It shows Δ for the case of (**b**) Cliff and (**c**) Spike at HTM/perovskite junction. Line in red shows the interfacial recombination. For reduced interfacial recombination value of Δ must be larger

suitable reason for the low recombination at slightly positive valence band offset is found to be the low value of Δ, which is the energy difference $E_{C\ Perovskites}$ -$E_{V\ HTL}$ (see Fig. 2). The cliff at the perovskite/HTL junction lowered the Δ shown in Fig. 2b, enhancing the chances of recombination of an electron from perovskite to hole from HTL. The presence of a spike at the junction increases the Δ value shown in Fig. 2c and thus lower the chances of recombination of an electron from perovskite and hole from HTL. The high Spike value will impede the hole transfer from perovskite to HTL. The small positive magnitude of the valence band offset (VBO) are advantageous and their optimum value can be ascertained by simulation. Device optimization by simulation for an HTL (*p*-layer) in *p-i-n* optimizing conditions are.

(i) A positive VBO at the *p-i* junction.
(ii) High hole density in *p, n* layer (p^+-*i* structure),

(a) High built-in voltage
(b) Lead to the higher field in the absorber (*i*) layer.

3.1 HTL parameter

For the simulation of inorganic HTL, we applied an interface defect layer (IDL) at the HTL perovskite junction. The width and defect density of IDL were taken to be 10 nm and 10^{17} cm^{-3}. The high defect density in IDL was used to simulate the interfacial recombination caused by lattice mismatching and defect state. In line to CZTS, which has a bandgap tail state of multivalent defect near to conduction band and valence band, we assumed multivalent defect of charge state {3+/2+, 2+/+,+/0} in conduction band (CB) at $E_t = 1.40$ eV with characteristic energy of 0.05 eV and acceptor defects of charge state {0/-, -/2-, 2-/3-} at valence band (VB). The defect density of 5×10^{14} cm^{-3}, capture a cross section of 10^{-13} cm^2. To model SnS defects we have used a neutral defect of density 10^{17} cm^{-3}. Energetic distribution of single level was 0.6 eV above E_V and capture cross-section of $10^{-15}cm^2$. The parameter of the CZTS, CIGS, Cu_2S, Sb_2S_3, PbS, FeS_2, SnS is taken from literature and are listed in Table 2.

These inorganic materials are *p*-type with 2–4 order high hole density than perovskite and have a similar bandgap. Simulation is run for these sulfides as HTL in Perovskite solar cell. HTL parameters of thickness, hole density are optimized by running simulation. Figure 3 shows the dependence of inorganic HTL device performance on hole density, thickness. The hole density in the HTL is varied from 10^{14} to 10^{18} cm^{-3} to simulate the effect on efficiency. Efficiency rises with hole density for all HTL. As doping concentration in HTL increases, the resistivity of the HTL layer reduces. This increases the V_{OC} and FF whereas the current remains constant. Volatge as a function of hole density is simulated in Fig. 3c which increase with hole density. Current remain same for increase in hole density as simulated in Fig. 3d. Carrier (hole) concentration will affect the bend banding and potential distribution at the junction. Perovskite has low doping thus higher doped HTL will induce banding in the Perovskite absorber layer thus creating a potential distribution across the perovskite layer. Higher carrier concentration will cause higher built-in voltage in the device and is favourable until limiting diffusion length at high carrier density, Auger and Radiative recombination effect supersedes. All the binary sulfides layers have shown 0.1 μm optimum thickness after which efficiency becomes constant. Quaternary CZTS and CIGS have shown a 0.2 μm as optimum thickness. With thickness, FF grows initially and

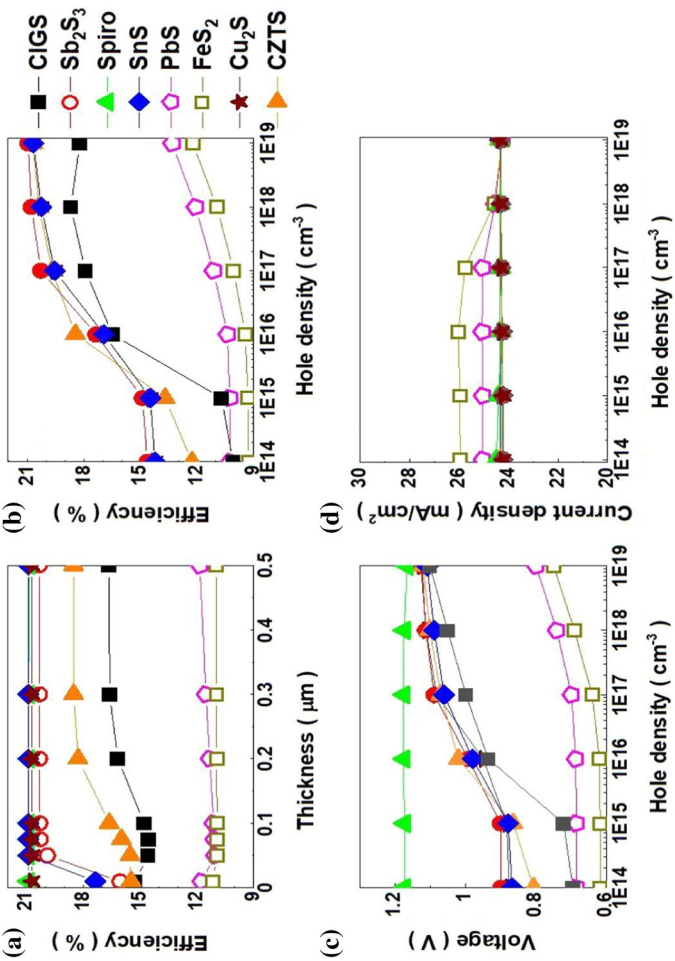

Fig. 3 **a** Efficiency vs thickness of the HTM layer is simulated. To obtain optimum HTM layer width of the various HTM/Perovskite solar cell. **b** Efficiency vs Hole density is plotted for all the HTL/perovskite cell. Higher hole density in HTL layer is preferred for high efficiency of inorganic HTM/perovskite cell. **c** The dependance of volatge on hole density for various HTL/perovskite devices. **d** Simulated dependeance of current on hole desnity for various HTL/perovskite devices

then all the parameter becomes constant. Rau et. al. estimated critical mobility for achieving 90% of efficiency in the solar cell (Mattheis et al. 2008). The critical mobility values remain less than 1 cm^2V^{-1} s^{-1}. HTL materials under consideration here well know *p*-type material with mobilities higher than critical mobilities as required by Rau et al. The optimum value of thickness, hole density as obtained by simulations can be easily attainable in given HTL materials. These parameters are highly dependent on growth condition and stoichiometry. We have used the value of these parameters to form the experimental data reported in the literature and listed in Table 2.

3.2 Band-diagram and I-V

The band structure of all the HTL/Perovskite solar cells are simulated and plotted in Fig. 4. A comparative band alignment at the HTL/perovskite junction was observed. The HTL layer energy level in the CZTS, CIGS has a bending due to hole density of 10^{16} cm^{-3}. Moreover, SnS showed band bending at the back metal contact. The simulated I-V curve of all the structure were shown in Fig. 5. The junction of HTL/perovskite is found to be dynamic. Contrary to, PbS and FeS_2 which shows a low efficiency of 11.1% and 10.9% due to a large negative VBO at HTL/perovskite junction, CIGS and CZTS have a moderate value of efficiency of 16.5% and 18.4% respectively and had a positive VBO of 0.25 and 0.15 eV. In addition, SnS, Cu_2S, Sb_2S_3 exhibits comparable efficiency to Spiro-MeOTAD perovskite solar cell at 20.88%, 20.6%, 20.2% respectively. The comparable efficiency of

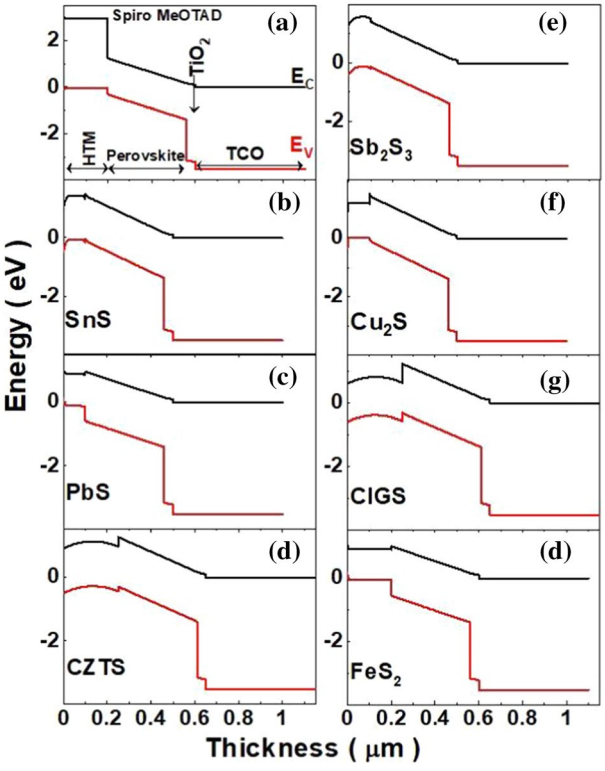

Fig. 4 Simulated band diagram showing energy level of various HTL/perovskite with respect to layer widths. Black line shows the conduction band and red line shows the valence band energy level. It brings out the comparative detail of the band alignment at various HTL/perovskite interface and suitable valence band offset (VBO) at the interface. **a** Spiro MeOTAD/Perovskite solar cell junction, **b** SnS/Perovskite solar cell junction, **c** PbS/Perovskite solar cell junction, **d** CZTS/Perovskite solar cell junction, **e** Sb_2S_3/Perovskite solar cell junction, **f** Cu_2S/Perovskite solar cell junction, **g** CIGS//Perovskite solar cell junction, **h** FeS_2/Perovskite solar cell junction. with the and inorganic HTL. The structure is identical for the TCO, TiO_2, Perovskite layers. Simulation bringout the valence band offset at perovskite/HTL junction and band bending profile in HTL for various HTL/perovskite cells

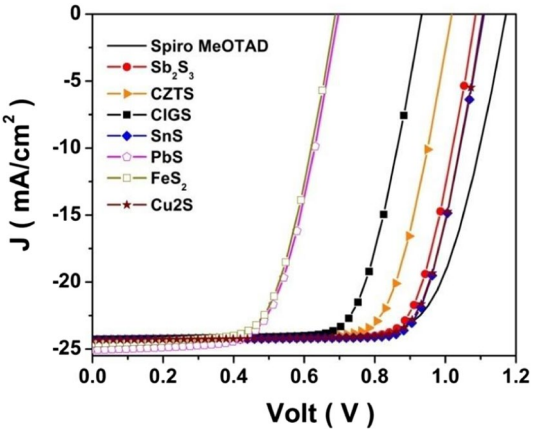

Fig. 5 J-V curve of the all inorganic HTL/perovskite solar cells

SnS could be further optimized, enhanced and could replace SpiroMEOTAD organic HTL. The difference in electron affinity (X_{HTL}) of the HTL layer and perovskite (X_{Abs}) causes the valence band offset (VBO) at the junction. However, for the hole transport VBO, alignment of the valence band level E_V of HTL and E_V of perovskite are the important parameters. VBO influence hole transfer from perovskite to HTL and is important parameter to control interfacial recombination. We have introduced a 10 nm thick layer (at the HTL junction, an interface defect density is assumed) at this junction to simulate defect arising from electrical or mechanical dissimilarity.

3.3 VBO and contact optimization of HTL layer

VBO is the discontinuity in the energy level at the junction shown by a vertical line in Fig. 2 and had been calculated by $(E_{gHTM}+X_{HTL})–(E_{gPerov.}+X_{Perov})$. Where, E_g is the bandgap and X is electron affinity. The obtained simulated band diagram of the device (inorganic HTL/Perovskite) showed a valence band offset. Moreover, the high negative offset introduces a cliff, favourable pathway for hole transport from perovskite to HTL case shown in Fig. 2b for Perovskite/SpiroMeOTAD. In addition, the high positive offset $(X_{HTL}+E_{gHTL}>X_{Abs}+E_{gAbs})$ introduces a spike leading to formation of a barrier for hole transfer from the absorber to HTL as shown in Fig. 2c. Thus, a zero valence band offset make continuity at the junction. The Δ value as shown in the figure is observed to be large to avoid interfacial recombination between $E_{V\ HTL}$ and $E_{C\ Perovskite}$. Therefore, the positive value of VBO is suitable to increase Δ. However large VBO will inhibit the hole transfer from the absorber to HTL and the height of the spike should be less than the built-in voltage in an absorber. SnS show comparable efficiency to Spiro, therefore, we optimized SnS for further efficiency enhancement. The electron affinity of the HTL layer is tuned to vary the VBO and the band alignment. The band alignment is simulated for positive and negative as well as for the zero valence band offset. SnS/perovskite found to have a E_{VBO} of 0.15 eV (see the band diagram in Fig. 4) and the effect of spike and cliff on the performance of the device performance is analyzed. The simulation was run for a range of VBO values including from negative to the positive value. The defect at the junction of perovskite/HTL was simulated by inserting an IDL (interface defect layer) with a defect density of 10^{17} cm^{-3}.

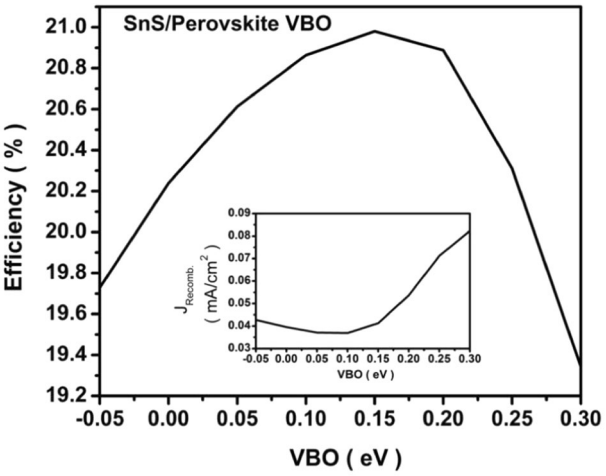

Fig. 6 VBO effect on the efficiency for the HTM(SnS)/Perovskite solar cell is plotted. Interface defect density 10^{17} cm^{-3} is used for SnS/perovskite case. Inset curve is showing the recombination current with respect to VBO. Efficiency is maximum and recombination current is (J_{rec}) is minimum for the slightly positive value of VBO

Table 4 FF variation with band alignment (VBO) at the SnS/perovskite junction

Electron affinity (eV)	VBO (eV)	FF (%)
3.8	− 0.01	75.33
3.9	0.0	76.98
4	0.1	77.67
4.1	0.2	77.24
4.15	0.25	76.14

The dependence of cell efficiency on VBO at the interface was shown in Fig. 6. For a VBO values of − 0.05–0.3 eV the efficiency increases and the intense peak was observed at a value of 0.15 eV. It is evident that the interface defect density at the junction highly affects the negative valence band. The recombination current is minimum at the slightly positive valence band offset region and its dependence on valence bands is shown in Fig. 6. The efficiency maximises in that VBO positive region, where the recombination current is also in its lowest values. The interfacial recombination is numerically lower in slightly positive VBO region. Moreover, the value of the recombination current depends upon the defect density at the interface. Therefoe, a high positive VBO is detrimental for performance as evident from the simulated results. A slightly positive band offset of 0.05 eV–0.1 eV will yield high efficiency irrespective of the high defect density for SnS. The reason behind the low value of the recombination current at a slightly positive valence band offset is the low value of Δ. It was observed that the efficiency of the device abruptly decreases for higher VBO values as seen in the simulation Fig. 6. This is attributed to the interfacial recombination within the HTL/Perovskite junction and can be lowered by a positive band offset. The marginal positive values of VBO are advantageous and their optimum value can be ascertained by simulation. The prominent effect of the VBO relies on the fill factor of the device. Table 4 summarises the VBO due to the variation of the electron affinity of SnS, while FF maximize at the marginal positive VBO (0.1 eV) and the similar trend was observed for the efficiency.

The band diagram of SnS/perovskite in Fig. 4 shows an abrupt band bending at the back contact and suggests a Schottky type back contact with the assumed metal contact work function of 5.1 eV in the simulation. To avoid this. the barrier at the back contact can be sorted by optimizing the back contact work function. Therefore, for contact optimization we simulated the effect of the work function (ϕ_m) on metal contact at the HTL layer. Figure 7 shows the efficiency improvement with the work function (ϕ_m) of back contact. Simulation results show that V_{OC} and efficiency rise initially with work function and then becomes constant for both the HTL shown in Fig. 7. This increase in V_{OC} is due to the improved built-in voltage (Rached and Mostefaoui 2008; Minemoto and Murata 2014). We have used a metal/semiconductor back contact acting as a Schottky barrier for the majority carrier and the barrier value is lowered to make it near as ohmic. The band diagram was simulated for increasing work function values. For higher work function there is a rise in the energy level of the HTL at the back contact. This rises in energy level at back contact improves built-in voltage in HTL and perovskite layer. The simulated band diagram is shown along with the work function in the inset of Fig. 7. The bending in E_V and E_C level at rear contact were eliminated with metal contact of high work function as shown in the simulated diagram.

The final parameters of the perovskite with the inorganic HTL layer are summarized in Fig. 8. The inorganic HTL (CZTS, Sb_2S_3, Cu_2S, SnS) have higher FF and SnS have higher efficiency than the standard perovskite cell with organic Spiro HTL. The V_{OC}, FF, J_{SC} and efficiency are compared with spiro-MeOTAD and the SQ limit. The SQ limit gap in V_{OC}, J_{SC}, FF for spiro-MeOTAD is shown. Among them FF has the largest deficit this may be due to suboptimal band alignment at the perovskite/HTL, perovskite/ETL and the high value of series resistance and low shunt resistance values in the perovskite solar cell. The efficiency of the SnS was observed to be higher than Spiro-MeOTAD. In addition, the thermal stability of SnS and low thermal conductivity makes it an advantageous material over organic HTL like PEDOT: PSS, Spiro-MeOTAD etc.

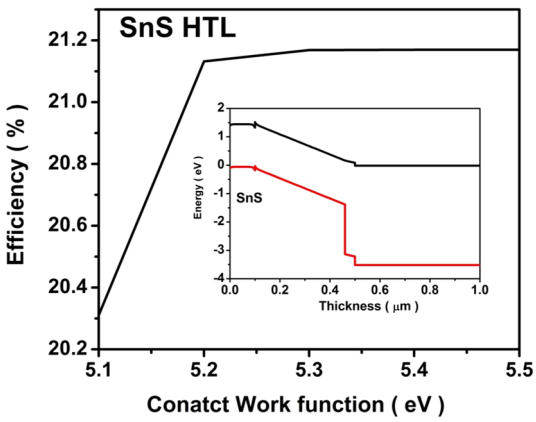

Fig. 7 Efficiency of the device with respect to the work function of the back metal contact. Band diagram at work function (ϕ_m) of the back metal contact is shown in the inset graph

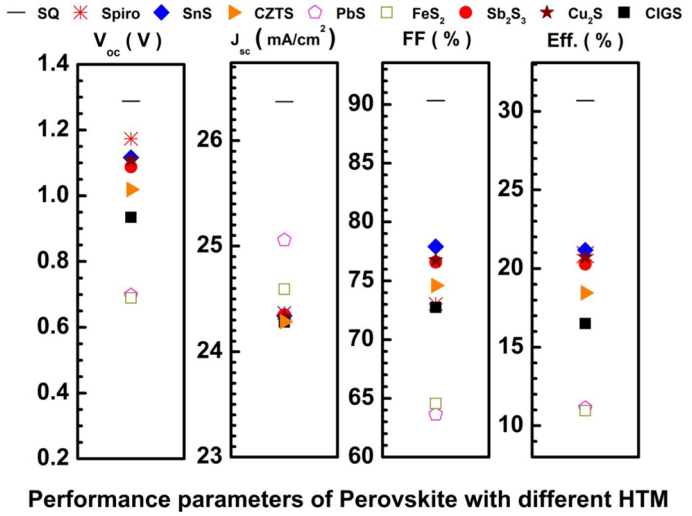

Fig. 8 The performance parameter of the Perovskite with Spiro-MeOTAD, chalcogenide HTM and SQ limit are compared. It shows the gap in SQ limit and present efficiency is primarily due to low FF factor and current of perovskite solar cells. Our suggested HTL layer has higher FF values than Spiro-MeOTAD

4 Conclusion

Earth-abundant inorganic HTL was used to provide insulation to the perovskite layer for enhanced stability and replacing costly, unstable organic HTM (Spiro-MeOTAD, PTAA etc.). Simulation results points out HTL property (a) small positive VBO at the HTL/perovskite junction and (b) high doping density. The inorganic chalcogenides SnS, p-type material have been explored for hole transport applications and are well suited for their availability, material stability and processability. Perovskite with inorganic HTL (Cu_2S, Sb_2S_3, SnS, CZTS, CIGS, FeS_2, PbS) are simulated shows high efficiency. A marginal positive VBO results to an efficiency of 20% which can be further improved with the flat band at the back contact. Our simulation result shows that SnS is a promising material and can effectively replace the organic Spiro-MeOTAD HTL with improved performance and stability.

Acknowledgements We gratefully acknowledgment Dr Marc Burgelman, Honorary Professor, University of Gent for providing SCAPS-1D software.

Declarations

Conflict of interest Authors declare they have no conflict of interest.

References

Altermatt, P.P., Kiesewetter, T., Ellmer, K., Tributsch, H.: Specifying targets of future research in photovoltaic devices containing pyrite ðFeS$_2$ Þ by numerical modeling. Solar Energy Mater. Solar Cells **71**, 181–195 (2002)

Burgelman, M., Nollet, P., Degrave, S.: Modelling polycrystalline semiconductor solar cells. Thin Solid Films **361–362**, 527–532 (2000)

Burton, A., Colombara, D., Abellon, R.D., Grozema, F.C., Peter, L.M., Savenije, T.J., Dennler, G., Walsh, A.: Synthesis, characterization, and electronic structure of single crystal SnS, Sn_2S_3, and SnS_2 L. Chem. Mater. **25**, 4908–4916 (2013)

Casas, G.A., Cappelletti, M.A., Cedola, A.P., Soucase, B.M., y Blanca, E.L.P.: Analysis of the power conversion efficiency of perovskite solar cells with different materials as hole-transport layer by numerical simulations. Superlattices Microstruct. **107**, 136–143 (2017)

De Angelis, A.D., Christian Kemp, K., Gaillard, N., Kim, K.S.: Antimony (III) sulfide thin films as a photoanode material in photocatalytic water splitting. ACS Appl. Mater. Interfaces **8**, 8445–8451 (2016)

Dhingra, P., Singh, P., Rana, P.J.S., Garg, A., Kar, P.: Hole-transporting materials for perovskite-sensitized solar cells. Energy Technol. **4**, 891–938 (2016)

Gokmen, T., Gunawan, O., Mitzi, D.B.: Minority carrier diffusion length extraction in Cu2ZnSn(Se, S)4 solar cells. J Appl Phys **114**, 114511 (2013)

Green, M.A., Emery, K., Hishikawa, Y., Warta, W., Dunlop, E.D., Levi, D.H., Ho-Baillie, A.W.Y.: Solar cell efficiency tables (version 49). Prog. Photovolt. Res. Appl. **25**, 3–13 (2017)

Hossain, M.I., Alharbi, F.H., Tabet, N.: Copper oxide as inorganic hole transport material for lead halide perovskite based solar cells. Sol. Energy **120**, 370–380 (2015)

Hwang, I., Jeong, I., Lee, J., Ko, M.J., Yong, K.: Enhancing stability of perovskite solar cells to moisture by the facile hydrophobic passivation. ACS Appl. Mater. Interfaces **7**, 17330–17336 (2015)

Kumar, A.: Efficiency enhancement of CZTS solar cells using structural engineering. Superlattices Microstruct. **153**, 106872 (2021a)

Kumar, A.: Numerical modelling of ion-migration caused hysteresis in perovskite solar cells. Opt. Quant. Electron. **53**, 1–9 (2021b)

Kumar, A., Ranjan, P.: Impact of light soaking on absorber and buffer layer in thin film solar cells. Appl. Phys. A **126**, 1–8 (2020)

Kumar, A., Ranjan, P.: Defects signature in V_{OC} characterization of thin-film solar cells. Sol. Energy **220**, 35–42 (2021)

Kumar, A.: Impact of selenium composition variation in CZTS solar cell. Optik **234**, 166421 (2021)

Lim, Y., Ok, Y.W., Tark, S.J., Kang, Y., Kim, D.: Electrical contact properties of Cu_2S nanowires grown vertically on Cu foil by gas–solid reaction. Curr. Appl. Physi. **9**, 890–893 (2009)

Lv, M., Zhu, J., Huang, Y., Li, Y., Shao, Z., Xu, Y., Dai, S.: Colloidal $CuInS_2$ quantum dots as inorganic hole-transporting material in perovskite solar cells. ACS Appl. Mater. Interfaces **7**, 17482–17488 (2015)

Mattheis, J., Werner, J.H., Rau, U.: Finite mobility effects on the radiative efficiency limit of pn-junction solar cells. Phys Rev B **77**, 085203 (2008)

Minemoto, T., Murata, M.: Impact of work function of back contact of perovskite solar cells without hole transport material analyzed by device simulation. Curr. Appl. Phys. **14**, 1428–1433 (2014)

Minemoto, T., Murata, M.: Theoretical analysis on effect of band offsets in perovskite solar cells. Sol. Energy Mater. Sol. Cells **133**, 8–14 (2015)

Mitzi, D.B., Gunawan, O., Todorov, T.K., Barkhouse, D.A.R.: Prospects and performance limitations for Cu–Zn–Sn–S–Se photovoltaic technology. Philos. Trans. r. Soc. A **371**, 20110432 (2013)

Popov, P.A., Fedorov, P.P., Kuznetsov, S.V.: Thermal conductivity of FeS2 pyrite crystals in the temperature range 50–300 K. Crystallogr. Rep. **58**, 319–321 (2013)

Qin, P., Tanaka, S., Ito, S., Tetreault, N., Manabe, K., Nishino, H., Nazeeruddin, M.K., Gratzel, M.: Inorganic hole conductor-based lead halide perovskite solar cells with 12.4% conversion efficiency. Nat. Commun. **5**, 1–6 (2014)

Rached, D., Mostefaoui, R.: Influence of the front contact barrier height on the Indium Tin Oxide/hydrogenated p-doped amorphous silicon heterojunction solar cells. Thin Solid Films **516**, 5087–5092 (2008)

Rau, U., Schock, H.W.: Electronic properties of Cu(In, Ga)S_e2 heterojunction solar cells–recent achievements, current understanding, and future challenges. Appl. Phys. A **69**, 131–147 (1999)

Shin, B., Gunawan, O., Zhu, Y., Bojarczuk, N.A., Chey, S.J., Guha, S.: Thin film solar cell with 8.4% power conversion efficiency using an earth-abundant Cu2ZnSnS4 absorber. Prog. Photovolt: Res. Appl. **21**, 72–76 (2013)

Skelton, J.M., Jackson, A.J., Dimitrievska, M., Wallace, S.K., Walsh, A.: Vibrational spectra and lattice thermal conductivity of kesterite-structured Cu_2ZnSnS_4 and $Cu_2ZnSnSe_4$. APL Mater. **3**(4), 041102 (2015)

Tang, Y.Q., Ge, Z.G., Feng, J.: Synthesis and thermoelectric properties of copper sulfides via solution phase methods and spark plasma sintering. Crystals. **7**(5), 141 (2017)

Wang, D., Wright, M., Elumalai, N.K., Uddin, A.: Stability of perovskite solar cells. Sol. Energy Mater. Sol. Cells **147**, 255–275 (2016)

Wei, L., Chen, J., He, Q., Teng, W.: Study of lattice thermal conductivity of PbS. J. Alloys Compd. **584**, 381–384 (2014)

Wu, Q., Xue, C., Li, Y., Zhou, P., Liu, W., Zhu, J., Dai, S., Zhu, C., Yang, S.: Kesterite Cu_2ZnSnS_4 as a low-cost inorganic hole-transporting material for high-efficiency perovskite solar cells. ACS Appl. Mater. Interfaces **7**, 28466–28473 (2015)

Xu, L., Deng, L., Cao, J., Wang, X., Chen, W., Jiang, Z.: Solution-processed Cu(In, Ga)(S, S_e)2, nanocrystal as inorganic hole-transporting material for efficient and stable perovskite solar cells. Nanoscale Res. Lett. **12**, 1–8 (2017)

Yang, W.S., Noh, J.H., Jeon, N.J., Kim, Y.C., Ryu, S., Seo, J., Seok, S.I.I.: High performance photovoltaic perovskite layers fabricated through intramolecular exchange. Science **348**, 1234–1237 (2015)

Yeon, D.H., Mohanty, B.C., Lee, S.M., Cho, Y.S.: Effect of band-aligned double absorber layers on photovoltaic characteristics of chemical bath deposited PbS/CdS thin film solar cells. Sci. Rep. **5**, 1–7 (2015)

You, J., Meng, L., Song, T., Guo, T., Yang, Y.M., Chang, W., Hong, Z., Chen, H., Zhou, H., Chen, Q., Liu, Y., Marco, N.D., Yang, Y.: Improved air stability of perovskite solar cells via solution-processed metal oxide transport layers. Nat. Nanotechnol. **11**, 75–51 (2016)

Yu, W., Li, F., Wang, H., Alarousu, E., Chen, Y., Lin, B., Wang, L., Hedhili, M.N., Li, Y., Wu, K., Wang, X., Mohammed, O.F., Wu, T.: Ultrathin Cu_2O as an efficient inorganic hole transporting material for perovskite solar cells. Nanoscale **8**, 6173–6179 (2016)